

Supplement of Atmos. Chem. Phys., 17, 14727–14746, 2017
<https://doi.org/10.5194/acp-17-14727-2017-supplement>
© Author(s) 2017. This work is distributed under
the Creative Commons Attribution 3.0 License.



Supplement of

Illustration of microphysical processes in Amazonian deep convective clouds in the gamma phase space: introduction and potential applications

Micael A. Cecchini et al.

Correspondence to: Micael A. Cecchini (micael.cecchini@gmail.com)

The copyright of individual parts of the supplement might differ from the CC BY 3.0 License.

Lagrangian model runs

Model runs were performed to confirm the overall directions of the displacements caused by the pseudo-forces defined in the paper. We identified that the ideal tool to address this issue would be a relatively simple model that solves the condensation and collision-coalescence growth using the bin approach instead of the bulk. A model that fits those requirements is described in Feingold et al. (1999) – item “c” in section 3, where we run only two parcels and not a bigger ensemble. This is a parcel model that treats the DSDs in 35 mass-doubling bins from 3.5 μm up to ~ 9 mm in diameter. The processes solved by the model are: 1) CCN activation (only at cloud base), considered to be composed of ammonium sulfate; 2) growth by condensation; 3) growth by collision-coalescence and 4) effects of giant CCN on the DSD evolution (we turn this process off for the purposes of this work). Other processes such as aqueous chemistry, complex aerosol composition, trace gases and radiation (and the effects of those processes on the DSDs) are not treated. Additionally, by being a parcel model, it does not consider turbulent mixing and sedimentation.

The characteristics of the model make it suitable to simulate the effects of condensation and collision-coalescence growth in the DSDs, which we can use to show the related patterns in the Gamma phase-space. We tried to produce results based on the conditions measured during flight AC09 (or RA1), where we used the following parameters as input: 1) aerosol mean geometric diameter $D_g = 1.55 \mu\text{m}$, with geometric standard deviation of 2.2 for the lognormal function of the aerosols; 2) pressure at cloud base of 890 hPa; and 3) temperature at cloud base of 20.85 $^{\circ}\text{C}$. The vertical speed was fixed at 0.5 m s^{-1} . Under those conditions, we ran the model twice: one run with only condensational growth (CG run) and one with both condensation and collision-coalescence growth (C2G run). Both runs produced the exact same DSDs in the lower parts of the cloud where the condensation dominates, but differed significantly when the collision-coalescence became active (around 1200 m, where cloud base is at 0 m). When the collision-coalescence process activates, $D_{eff} \approx 25 \mu\text{m}$ and the condensational growth is much less effective. Therefore, it was possible to isolate both processes. Because there is no turbulent mixing or dilution with

dry air, the droplet growth with altitude is much more pronounced in the model compared to our measurements during AC09. For this reason, we do not limit the Gamma fit to $D < 50 \mu\text{m}$ as in the paper. Otherwise, it would be difficult to capture the effects of the collision-coalescence process – droplets grow relatively quickly beyond the $50 \mu\text{m}$ mark.

We fitted Gamma DSDs (using the same moments of order zero, two, and three as in the paper) to the model outputs every 20 seconds. Therefore, each point in the Gamma phase space represents the instantaneous DSD measured every 20 seconds. The results are shown in the following three figures.

Figure S1 shows the Gamma phase space for both runs, where “*” markers are related to CG and squares to C2G. The arrows represent the displacement vector every 20 seconds, which is related to the respective pseudo-force (colors represent altitude above cloud base in m). Note that in the first 500 m the Gamma points are exactly the same for both runs. This layer is defined by condensational growth alone and we observe a “zig-zag” pattern in the Gamma phase-space. When the trajectory is upwards in the “zig-zag”, they are similar to what we observed in the paper – that is, growing μ and λ (and shrinking N_0) along with the condensational growth. On the other hand, the model results also show a downward trend during condensational growth. We noted that when the trajectory is downwards, the Gamma fit does not represent the DSD width correctly. At those points, the fixed bins between $10 \mu\text{m}$ and $15 \mu\text{m}$ present fast-growing concentrations (when the droplets grow sufficiently to transition from the lower bins) that disproportionately affects the Gamma DSD width. In the downward pattern, the Gamma DSD relative dispersion can be up to 150% higher than the binned DSD. When the process stabilizes, the trajectory returns to the upward trend and the Gamma and binned DSD widths get progressively closer (~20% to ~50% difference). Because of this, it is safe to conclude that the condensational growth in the model produces trajectories in similar directions to what we observed in the paper.

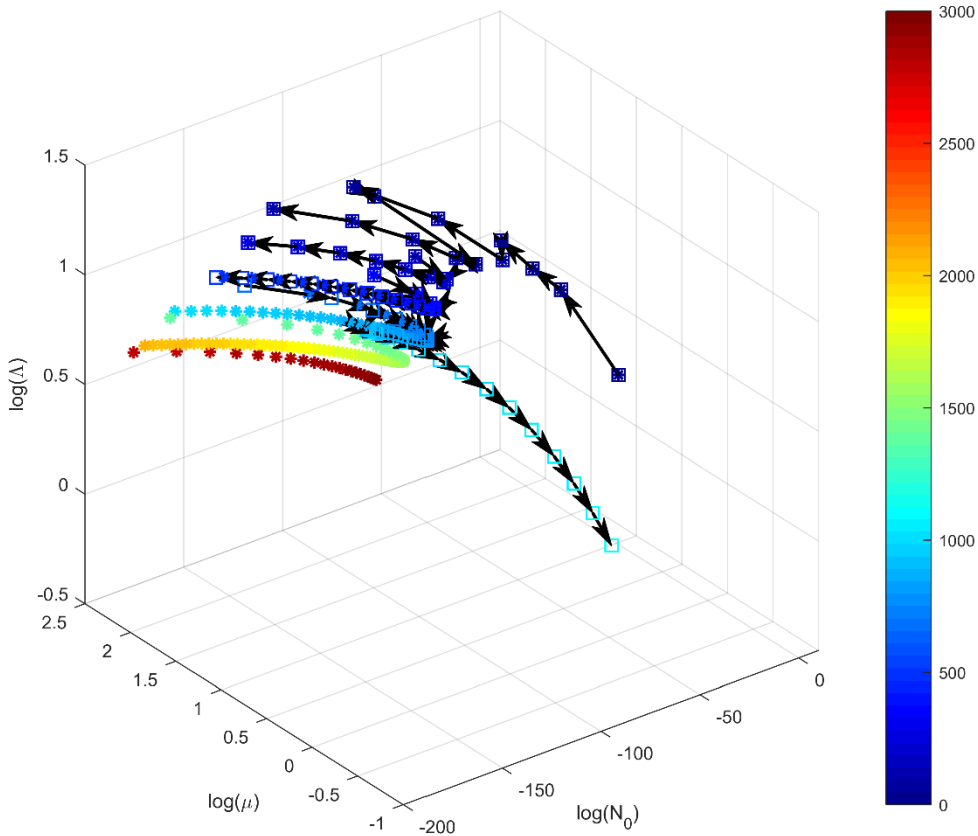


Figure S1: Gamma phase-space for both CG and C2G runs. The “*” markers are relative to the CG run, while squares represent the C2G run. Arrows represent the displacement vector between each 20-s point, which is related to the respective pseudo-force. Colors represent altitude above cloud base in m.

Figure S2 shows the same points of Figure S1, but colored according to D_{eff} . Additionally, we show lines of constant D_{eff} along a surface (not shown) of $N_d = 250 \text{ cm}^{-3}$ similarly to Figure 10 in the paper. The lines start at $5 \text{ }\mu\text{m}$ in the top and grow in $5 \text{ }\mu\text{m}$ intervals up to $50 \text{ }\mu\text{m}$ in the bottom line. When comparing the trajectories with the D_{eff} lines, it is possible to see where the droplets are growing faster. For instance, the condensational growth close to cloud base is very effective (because the droplets are smaller) and the trajectory tend to cross the D_{eff} lines. However, when droplets reach $D_{eff} \approx 25 \text{ }\mu\text{m}$, the trajectories get almost parallel to the lines, showing slower growth. On the other hand, the collisional growth accelerates

with increasing De_{eff} . This is expected from theory, but it is interesting to quantify its effects on the spherical coordinates of the displacement vectors – Figure S3.

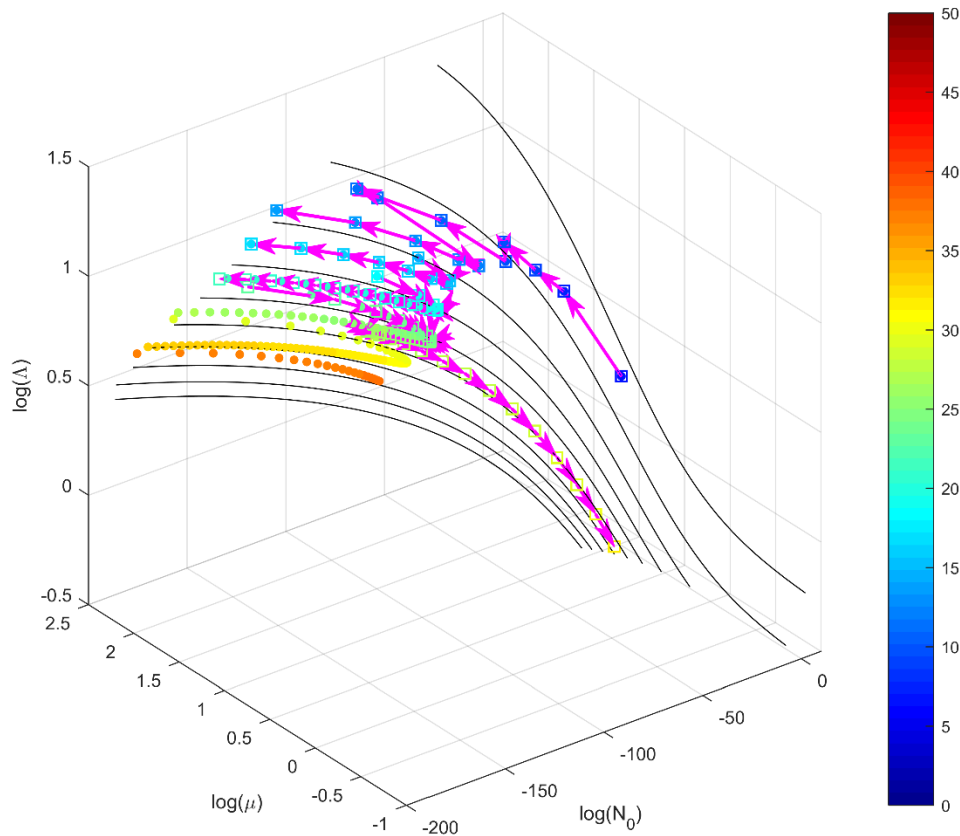


Figure S2: similar to Figure S1, but colored according to D_{eff} . The lines shown are lines of constant D_{eff} along a surface of $N_d = 250 \text{ cm}^{-3}$ as in Figure 10 in the paper, going from $5 \mu\text{m}$ (top line) to $50 \mu\text{m}$ (bottom line) – $5 \mu\text{m}$ intervals.

Figure S3 shows the spherical coordinates of the vectors in Figures S1 and S2. θ is the azimuth angle measured in the plane $\log(N_0) \times \log(\mu)$, being 0 at the $\log(N_0)$ axis and growing counter-clockwise. φ is the elevation angle, measured from the plane $\log(N_0) \times \log(\mu)$ towards the $\log(\Lambda)$ axis. The size of the vectors is measured by r . In Figure S3 we excluded the points in the downward part of the “zig-zag”

mentioned above. Non-filled circles in Figure S3 represent condensational growth alone, while filled markers represent collision-coalescence (colors are altitude above cloud base in m). It is possible to note that the elevation angle φ is slightly positive for the condensational growth, decaying with D_{eff} . The average value of this angle is 0.26° . It has small values mainly because of the bigger values of $\log(N_0)$ as compared to $\log(A)$. Nonetheless, the most important feature is its sign transition from condensational to collisional growth. On the latter, the angle seems to grow linearly with D_{eff} (except for the last point) as the process intensifies – averaged value of -4.23° . Overall, this angle is related to the DSD curvature trend – positive when the curvature is shrinking (condensational growth) and negative when the curvature is increasing (collisional growth).

The azimuth angle θ defines how N_0 and μ evolve along the trajectory. For the condensational growth, this angle averages 179.6° , meaning growing $\log(\mu)$ and shrinking $\log(N_0)$. On the other hand, this angle averages -13.7° for collisional growth and results in the opposite trend for the parameters. Both observations are in line with what we observed in the paper – now there is at least some quantification of the angles. Note that the angles most likely have different values in our observations given the differences in the values of the Gamma parameters. However, their sign, and therefore the direction of the motion in the space, is the same between our model calculations and the observations shown in the paper. Finally, we can note that r tends to decrease as the condensation rates decay, but it does not increase as the collisional growth intensifies. However, the acceleration of the collisional growth is reflected in φ and θ – both decrease, resulting in a trajectory that crosses the D_{eff} lines in Figure S2.

Overall, the modeling results presented here clearly indicate that the patterns observed in the Gamma phase space in the paper are indeed related to the condensation and collision-coalescence processes. The relation between both processes and the evolution of the Gamma parameters are consistent between the Lagrangian simulation and the observations. The natural next step would be to calculate the speeds and accelerations (and therefore the actual pseudo-forces), but this will not be addressed in this introduction paper. The actual implementation of the concepts presented here would need further work that is beyond the scope of the present study.

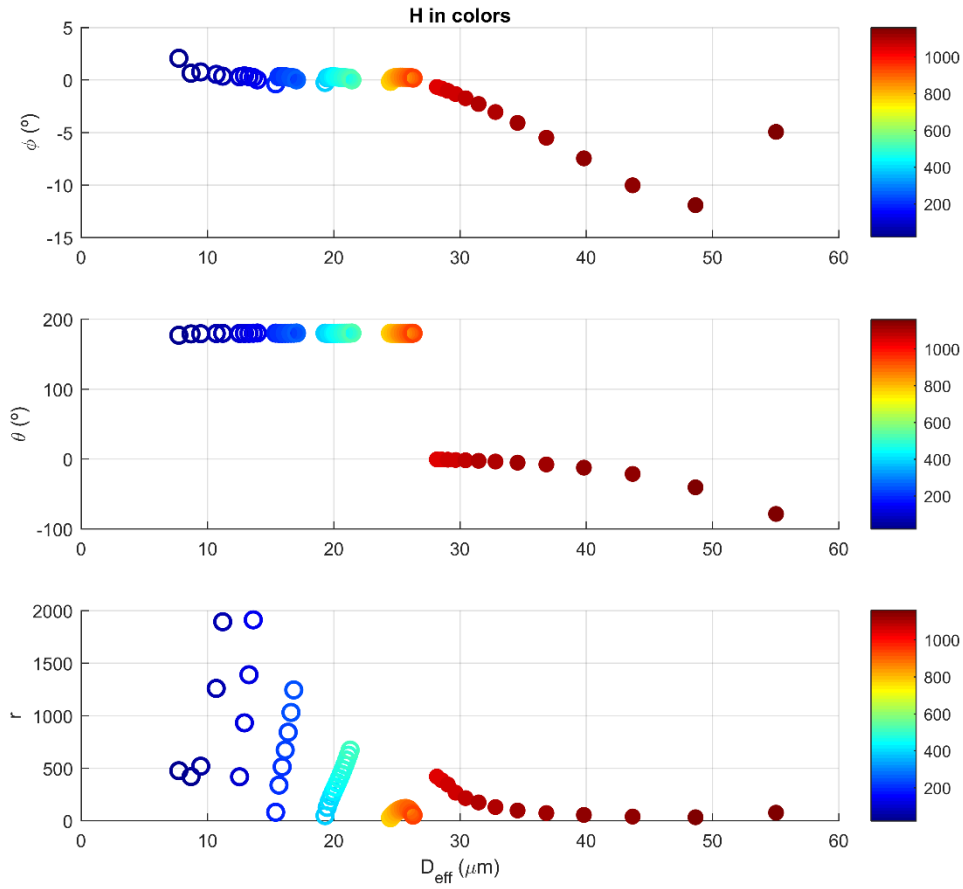


Figure S3: spherical coordinates of the displacement vectors shown in Figures S1 and S2. θ is the azimuth angle in the $\log(N_\theta) \times \log(\mu)$ plane, growing counter-clockwise (is 0 at the $\log(N_\theta)$ axis). ϕ is the elevation angle from the $\log(N_\theta) \times \log(\mu)$ towards the $\log(A)$ axis and r is the size of the vectors. The colors represent altitude above cloud base in m.

Effects of using other moments for the Gamma fits

We tested a new fit based on moments of order 3, 4, and 6 (M346). Here we reproduce Figures S1-3 with this new approach (Figures S4-6). For this case, we had to limit the fittings to $D < 150 \mu\text{m}$ because of the stronger weight to bigger droplets that caused negative values of μ . Note that the patterns in the phase-space are very similar to the previous case (M023). Averaged values for θ and φ are 179.5° and 0.35° for condensation and -19.4° and -4.0° for collision-coalescence, respectively.

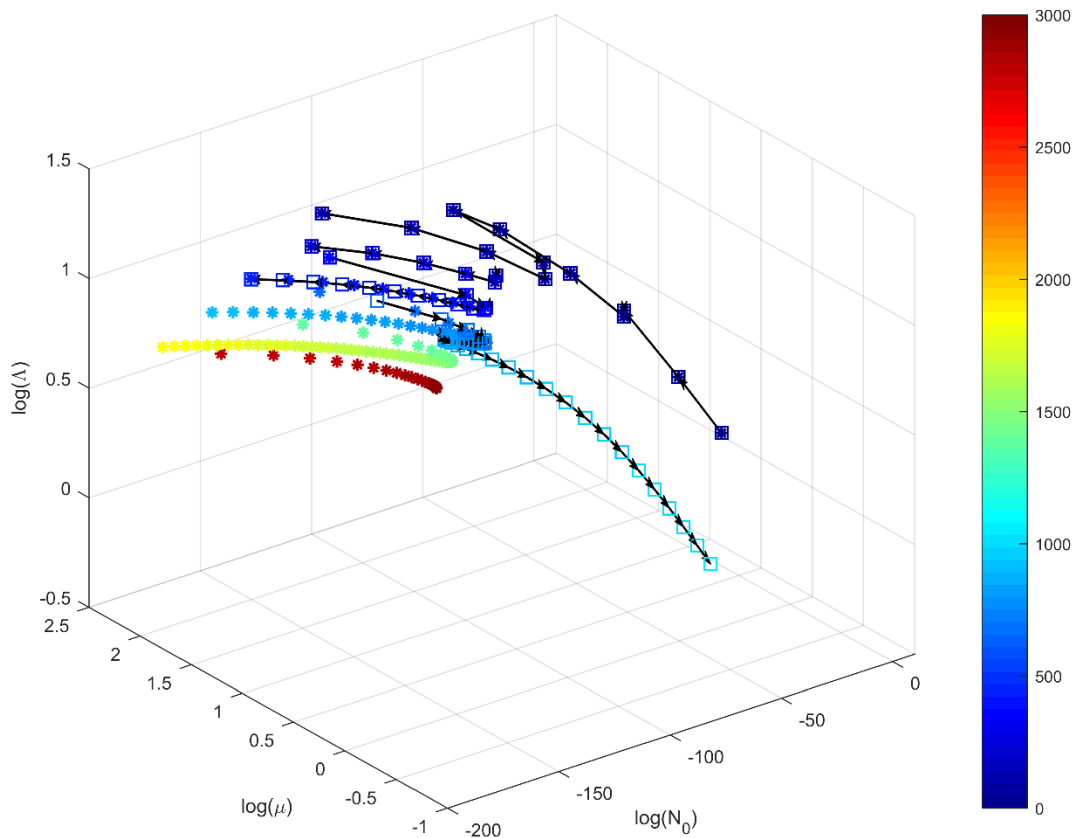


Figure S4: same as Figure S1, but for M346.

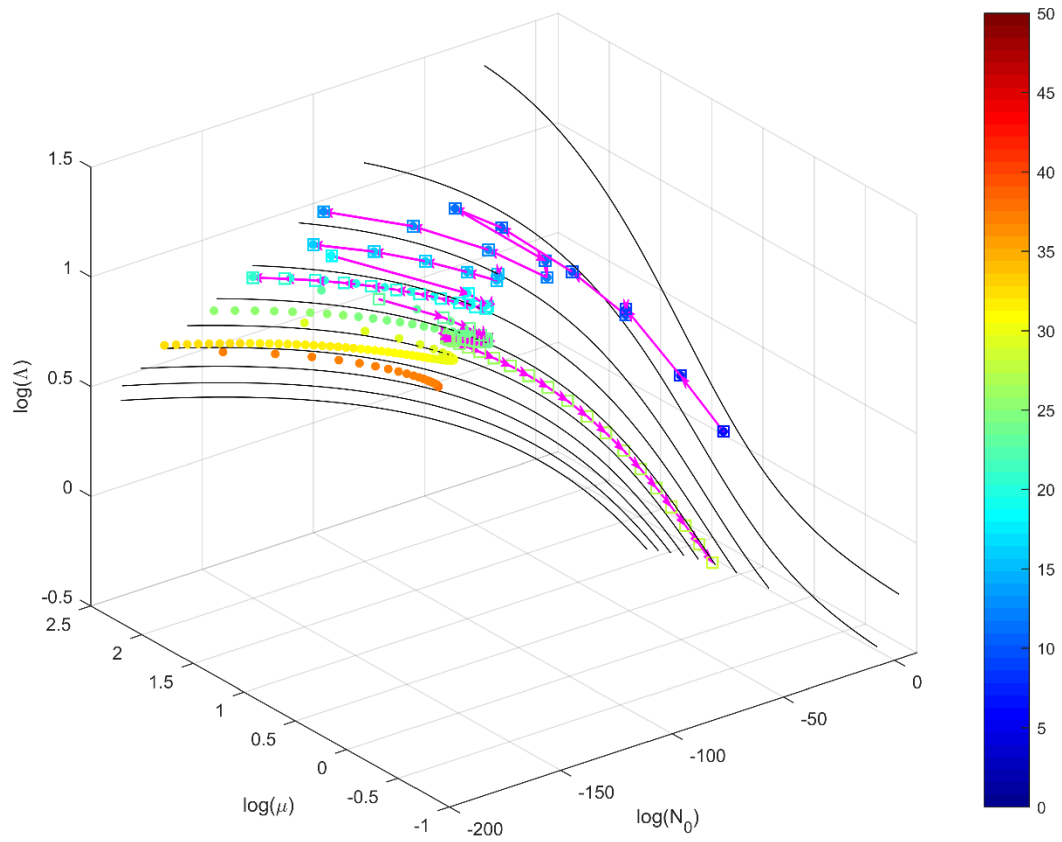


Figure S5: same as Figure S2, but for M346.

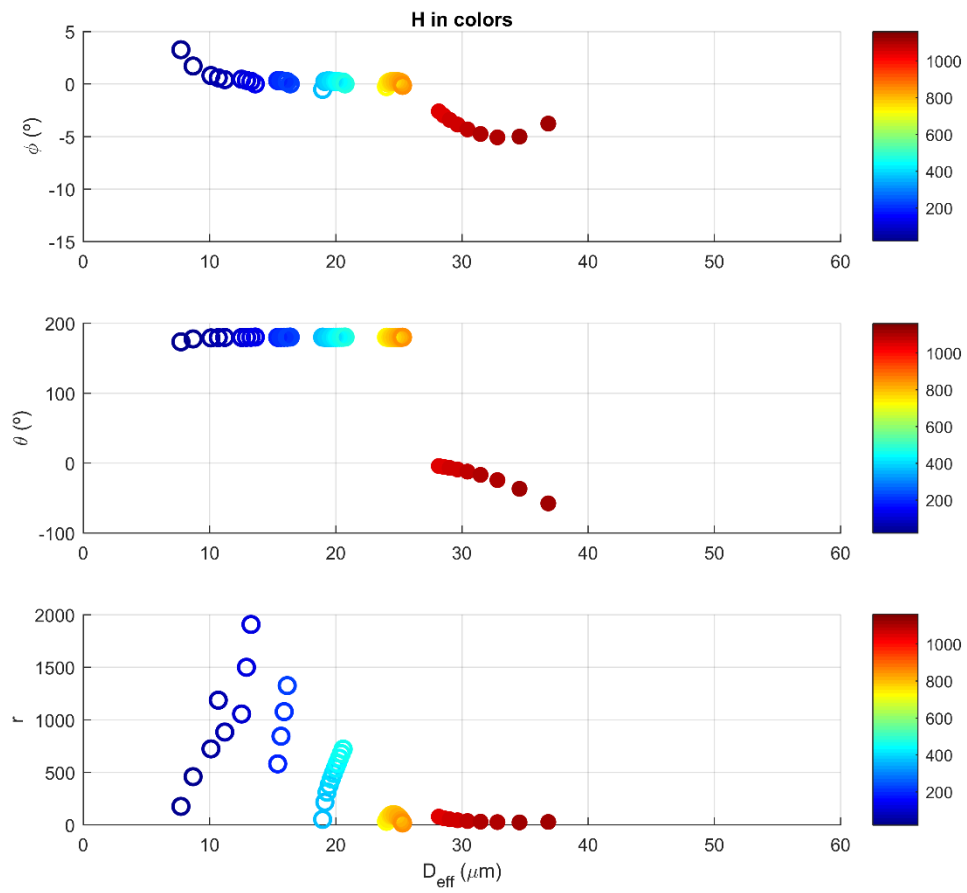


Figure S6: same as Figure S3, but for M346.